Brain, Behavior, and Immunity 105 (2022) 1–14

Contents lists available at ScienceDirect

Brain Behavior and Immunity

journal homepage: www.elsevier.com/locate/ybrbi

Full-length Article

# Blocking immune cell infiltration of the central nervous system to tame Neuroinflammation in Amyotrophic lateral sclerosis

Stefano Garofalo [a,*], Germana Cocozza [b], Giovanni Bernardini [c], Julie Savage [d], Marcello Raspa [e], Eleonora Aronica [f], Marie-Eve Tremblay [d], Richard M. Ransohoff [g], Angela Santoni [b], Cristina Limatola [b,h,*]

[a] Department of Physiology and Pharmacology, Sapienza University of Rome, Rome, Italy
[b] IRCCS Neuromed Pozzilli, Italy
[c] Department of Molecular Medicine, Laboratory Affiliated to Istituto Pasteur Italia, Sapienza University of Rome, Rome, Italy
[d] Division of Medical Sciences, University of Victoria Victoria, Canada
[e] EMMA CNR, Monterotondo, Italy
[f] Amsterdam UMC Location University of Amsterdam, Department of (Neuro)Pathology Amsterdam Neuroscience, Meibergdreef 9, Amsterdam, the Netherlands
[g] Third Rock Ventures, Italy
[h] Department of Physiology and Pharmacology, Sapienza University, Laboratory affiliated to Istituto Pasteur, Italia

ARTICLE INFO

*Keywords:*
Amyotrophic lateral sclerosis
Immune cells
Inflammation
Astrocytes
Microglia

ABSTRACT

Neuroinflammation is one of the main hallmarks of amyotrophic lateral sclerosis (ALS). Recently, peripheral immune cells were discovered as pivotal players that promptly participate in this process, speeding up neurodegeneration during progression of the disease. In particular, infiltrating T cells and natural killer cells release inflammatory cytokines that switch glial cells toward a pro-inflammatory/detrimental phenotype, and directly attack motor neurons with specific ligand-receptor signals. Here, we assessed the presence of lymphocytes in the spinal cord of sporadic ALS patients. Furthermore, we demonstrate that blocking the extravasation of immune cells in the central nervous system using Natalizumab (NAT), an antibody for the α4 integrin, reduces the level of interferon-γ in the spinal cord of ALS mouse models, such as the hSOD1$^{G93A}$ and TDP43$^{A315T}$ mice, modifying microglia and astrocytes phenotype, increasing motor neuron number and prolonging the survival time. Taken together, our results establish a central role for the immune cells as drivers of inflammation in ALS.

## 1. Introduction

Amyotrophic lateral sclerosis (ALS) is a progressive neurodegenerative disease characterized by the death of motor neurons (MNs) in the cerebral cortex, brain stem, and spinal cord. Most studies have focused on genetic forms of ALS, which represent about 20% of cases, leaving the remaining 80% of sporadic ALS (sALS) less investigated. Due to the multifactorial and complex nature of the mechanisms underlying neurodegeneration, the pathological features of ALS remain, to date, widely unknown. Among that, inflammation is one of the most striking hallmarks of both sporadic and familial forms of ALS (Liu and Wang, 2017). Evidence for inflammation have been observed in patients as well as in animal models, being characterized by the infiltration of peripheral lymphocytes, natural killer (NK) cells and macrophages, by the reactivity of astrocytes and microglia, and the overproduction of inflammatory cytokines (Vahsen et al., 2021; Béland et al., 2020; Clarke and Patani, 2020; Peric et al., 2017). Several therapeutic agents have been developed to inhibit or reduce inflammation in ALS affected regions, albeit unfortunately, no approach successfully increases the mean survival time of patients by more than few months (Liu and Wang, 2017; Vahsen et al., 2021).

Microglia and astrocytes are key regulators of the inflammatory response that occurs in ALS pathogenesis. Studies in patients and transgenic mice have revealed that microglial cells acquire a dual phenotype, depending on the stage of disease: the first protective/anti-inflammatory response turns with time into a toxic/pro-inflammatory

*Abbreviations:* NAT, Natalizumab; ALS, Amyotrophic Lateral Sclerosis; il-1b, Interleukin-1 beta; tnf-a, Tumor necrosis factor alpha; nf-kb, nuclear factor-kappa B; Sod1, superoxide dismutase 1; TDP43, TAR DNA-binding protein 43; VLA4, very late antigen-4.

* Corresponding authors at: Department of Physiology and Pharmacology, Sapienza University.
*E-mail addresses:* stefano.garofalo@uniroma1.it (S. Garofalo), cristina.limatola@uniroma1.it (C. Limatola).

https://doi.org/10.1016/j.bbi.2022.06.004
Received 31 January 2022; Received in revised form 29 April 2022; Accepted 5 June 2022
Available online 7 June 2022

phenotype (Clarke and Patani, 2020; Beers and Appel, 2019). The late-stage microglia favor inflammation and promote cytotoxicity via nuclear factor-kappa B (NF-kB) signals (Frakes et al., 2014) and by secreting reactive oxygen species and pro-inflammatory cytokines (such as interleukin (IL)-1, IL-6, tumour necrosis factor (TNF)-α), ultimately enhancing MN death (Beers and Appel, 2019; Thonhoff et al., 2011; Guidotti et al., 2021; Parisi et al., 2013). Moreover, in a subgroup of familial ALS (fALS) patients, expressing mutant superoxide dismutase 1 (SOD1), and in the corresponding mouse models, microglia affected MN death (McGeer and McGeer, 2002; Beers, 2011), promoted neurotoxicity (Beers et al., 2006; Boillée et al., 2006), as well as regulated the feeding behavior and overall metabolism (Cocozza et al., 2021). In line with these observations, the expression level of mutant SOD1 in microglia correlates with the late phase of ALS (Boillée et al., 2006). Similar results were obtained in a different transgenic model which expresses a mutated TAR-DNA binding protein and accumulates pathologic aggregates of ubiquitinated proteins in specific neurons, resulting in astrocytes and microglia reactivity and the loss of both upper and lower MN (Wegorzewska et al., 2009).

A phenotype of "dark" microglia has been identified in several pathologies and neurodegenerative diseases, such as chronic stress, aging, and Alzheimer's disease, being almost absent under steady-state conditions in mice (Bisht et al., 2016). Dark microglial cells exhibit several markers of oxidative stress, including mitochondrial alterations, but also a condensed, electron-dense cytoplasm and nucleoplasm that result in a dark appearance in electron microscopy, accompanied by remodeling of their nuclear chromatin (Nahirney and Tremblay, 2021; St-Pierre et al., 2020). Dark microglia appear to be much more active than other microglia, displaying numerous phagocytic inclusions, while making extensive direct contacts with neuronal elements (i.e., synaptic clefts, axon terminals, dendritic spines) with their highly ramified processes, suggesting a key implication in pathological tissue remodeling (Bisht et al., 2016). To date there is no description of dark microglia in ALS.

The contribution of astrocytes to ALS pathophysiology has been principally addressed by the use of animal models and *post-mortem* human tissue analyses. At ALS onset, astrocytes change their shape and molecular patterns, turning into reactive or activated astrocytes. Astrogliosis has been described, *post-mortem*, in the brain and near the MN soma in the spinal cord of sporadic and familial ALS patients (Kang et al., 2013). Of note, astrocyte-restricted expression of mutant SOD1 in mice failed to reproduce the neurodegenerative and inflammation phenotypes of ALS pathology (Haidet-Phillips et al., 2011), while the ablation of astrocytic mutant SOD1 transgene in mice significantly slowed disease progression and extended survival times (Gong et al., 2000), highlighting a fundamental role for the interaction between MNs and astrocytes in disease progression. Several studies reported impaired homeostatic function of astrocytes in ALS, such as defect in glutamate uptake due to the loss of the EAAT2 transporter, in sporadic and familial ALS patients and SOD1 mice (Wang et al., 2011). Astrocyte mitochondrial function is also compromised in ALS, together with defects in the cellular shuttling of lactate between astrocytes and MNs (Foran et al., 2011; Hounoum et al., 2017; Allen et al., 2019).

In this scenario, accumulating evidence implicate infiltrated peripheral immune cells as exerting deleterious effects on MN survival depending on the stage of pathology (Vahsen et al., 2021; Béland et al., 2020). $CD8^+$ T and the NK cells infiltrate the central nervous system (CNS) affected regions in ALS, directly killing the MNs via the recognition of specific proteins expressed by the damaged neurons (Garofalo et al., 2020; Coque et al., 2019). Additionally, T cells, NK cells and peripheral macrophages release pro-inflammatory cytokines which promote inflammation and switch glial cells toward a pro-inflammatory phenotype, starting from an early stage of pathology (Garofalo et al., 2020; Coque et al., 2019; Liu et al., 2020; Endo et al., 2015; Philips and Robberecht, 2011; Chiot et al., 2020). Recent studies also reported that the depletion of NK cells or macrophages in $hSOD1^{G93A}$, $hSOD1^{G37R}$ and $TDP43^{A315T}$ mice induces microglia to assume a protective state, enhancing the expression of neurotrophic factors, such as brain-derived neurotrophic factor (BDNF) (Garofalo et al., 2020, Chiot et al., 2020). Together these results highlight a participation of immune cells driving inflammation in ALS progression.

Despite all these studies supporting the involvement of the immune system in ALS progression in mouse models, to date, there are few evidence on the presence of infiltrated lymphocytes in the CNS of sporadic or familial patients (Troost et al., 1989; Kawamata et al., 1992; Engelhardt et al., 1993). Here, we demonstrate that $CD3^+$, $CD4^+$ and $CD8^+$ T cells infiltrate the spinal cord of sALS patients, and that only $CD8^+$ T cells directly contact MNs.

Since leucocytes use the α 4 integrin to cross the endothelial barrier for extravasation, we exploited the effect of Natalizumab (NAT), a blocking antibody for the α4 integrin (anti-VLA-4) (Yu et al., 2013; Gan et al., 2012), to reduce the transfer of peripheral immune cells to the CNS of two ALS mouse models. Our data show that, in the absence of infiltrating immune cells, there is a significant decrease of IFN- γ level in the spinal cord of $hSOD1^{G93A}$ and $TDP43^{A315T}$ mice, together with the acquisition of an anti-inflammatory phenotype by astrocytes and microglia. Furthermore, treating mice with NAT significantly enhanced their survival time, reducing the severity and delaying the insurgence of motor symptoms.

All these data establish the peripheral immune cells as key actors driving inflammation in ALS, suggesting that the blockade of immune cell infiltration in the CNS could represent a promising approach to contrast disease progression.

## 2. Results

### 2.1. Lymphocytes infiltrate the spinal cord of sALS patients.

To evaluate the possible role of peripheral immune cells in ALS, we first investigated the presence of $CD3^+$, $CD8^+$ and $CD4^+$ T cells in *post-mortem* sections of the spinal cord from sALS patients (listed in Table S1). In these tissues, the mean distance of $CD3^+$ T cells from blood vessels was 124.38 ± 30.6 μm, suggesting lymphocytes infiltration within the spinal cord parenchyma (Fig. 1A). Furthermore, we detected the presence of $CD4^+$ and $CD8^+$ T cells in the spinal cord from sALS patients, while they were not observed in the tissues from control individuals (Fig. 1B, C). Notably, only $CD8^+$ T cells showed structural contacts with MNs (Smi32 + cells) (Fig. 1D), while no contacts were observed between $CD4^+$ T cells and MNs (Fig. 1E).

### 2.2. Infiltrated peripheral immune cells shape microglial phenotype in the lumbar spinal cord.

We have previously demonstrated that, in $hSOD1^{G93A}$ mice, the IFN-γ released by infiltrating NK cells induced a pro-inflammatory microglial phenotype starting in an early phase of the disease (13 weeks) (Garofalo et al., 2020). To provide further insights into microglial phenotype in $hSOD1^{G93A}$ mice, we performed RNA sequencing (RNA-seq) of the microglial population isolated from the lumbar spinal cord of 16 weeks old mice and observed and increased expression of genes involved in glutamatergic and GABAergic neurotransmission, RNA transport, as well as protein degradation and digestion, in comparison to non-tg microglia (Fig. 2A–C), confirming the overexpression of inflammation-related genes (Chiu et al., 2013). Furthermore, as described for other neuropathological conditions (Bisht et al., 2016; Nahirney and Tremblay, 2021; St-Pierre et al., 2020), we described the presence of dark microglial cells within the spinal cord of $hSOD1^{G93A}$ mice (16 weeks old), but not in age-matched control non-tg animals (Fig. 2D). We reported that dark microglia extensively interact with myelinated axons (Fig. 2D), suggesting a possible involvement with the changes in myelination during ALS pathology (Gong et al., 2000) worth of further investigation.

To investigate if the infiltrating peripheral immune cells contribute

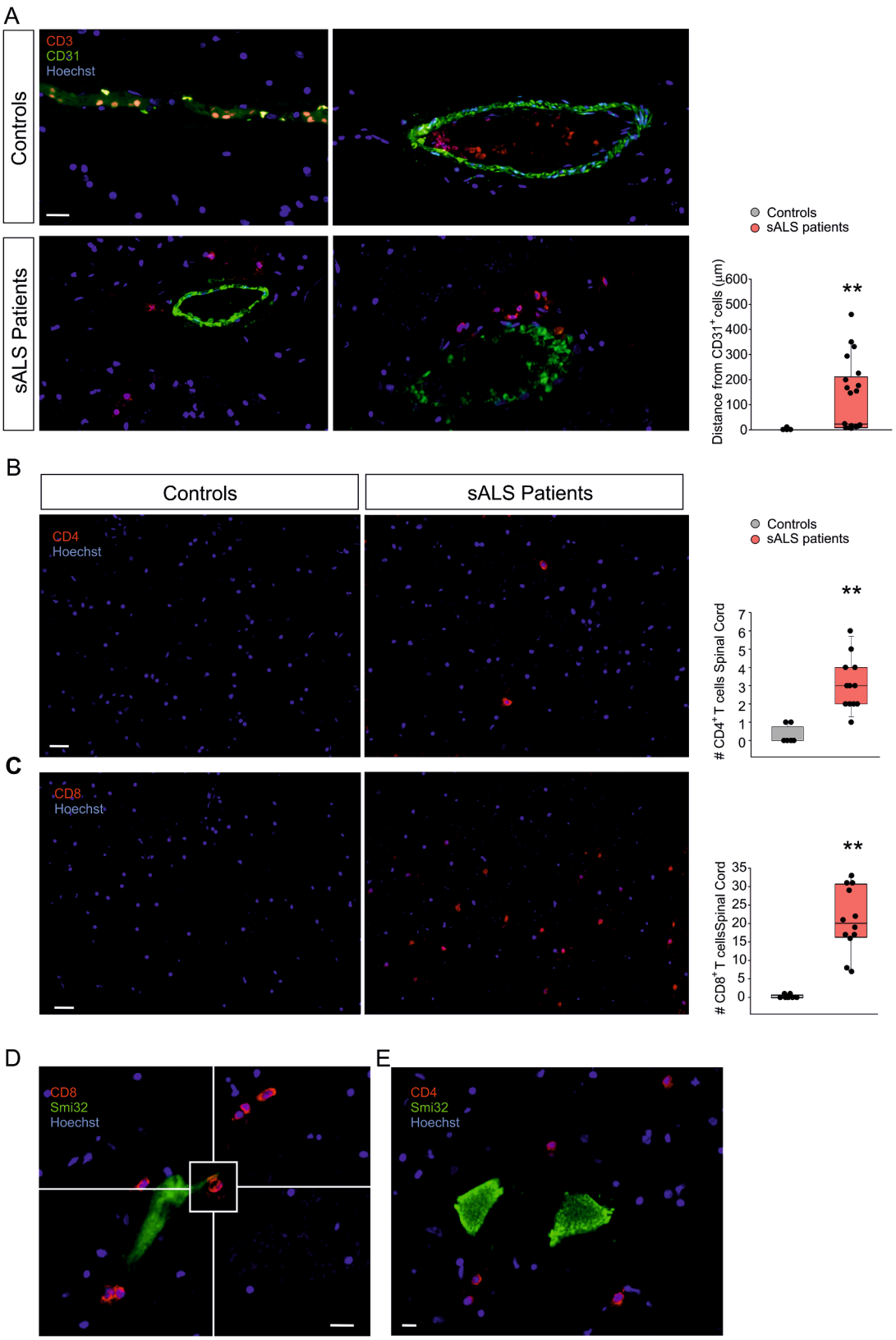


**Fig. 1.** Lymphocytes infiltrate the CNS affected regions in ALS patients. A) Distances of $CD3^+$ T cells from vessel (endothelial, $CD31^+$ cells) in the spinal cord of sALS patients (n = 12) and Controls (n = 8). **P < 0.001 two-tailed Student's *t*-test. Scale bar: 50 µm. Representative immunofluorescence is shown. Each dot represents the number of cells per section. B, C) $CD4^+$ (B) and $CD8^+$ (C) T cells (in red) in slices of spinal cord from sALS patients, absent in healthy subjects. Scale bar: 50 µm. (n = 8 controls, 12 sALS patients **P < 0.001 two-tailed Student's *t*-test). Each dot represents the number of cells per section. D, E) Representative images of $CD4^+$ and $CD8^+$ cell–MN contacts in the spinal cord of sALS patients (original magnification, x600). Scale bar: 20 µm. (n = 8 patients, at least 3 $CD8^+$ T cell-MN contacts per patient). For boxplots the center line, boxes and whiskers represent the median, inner quartiles, and rest of the data distribution, respectively.

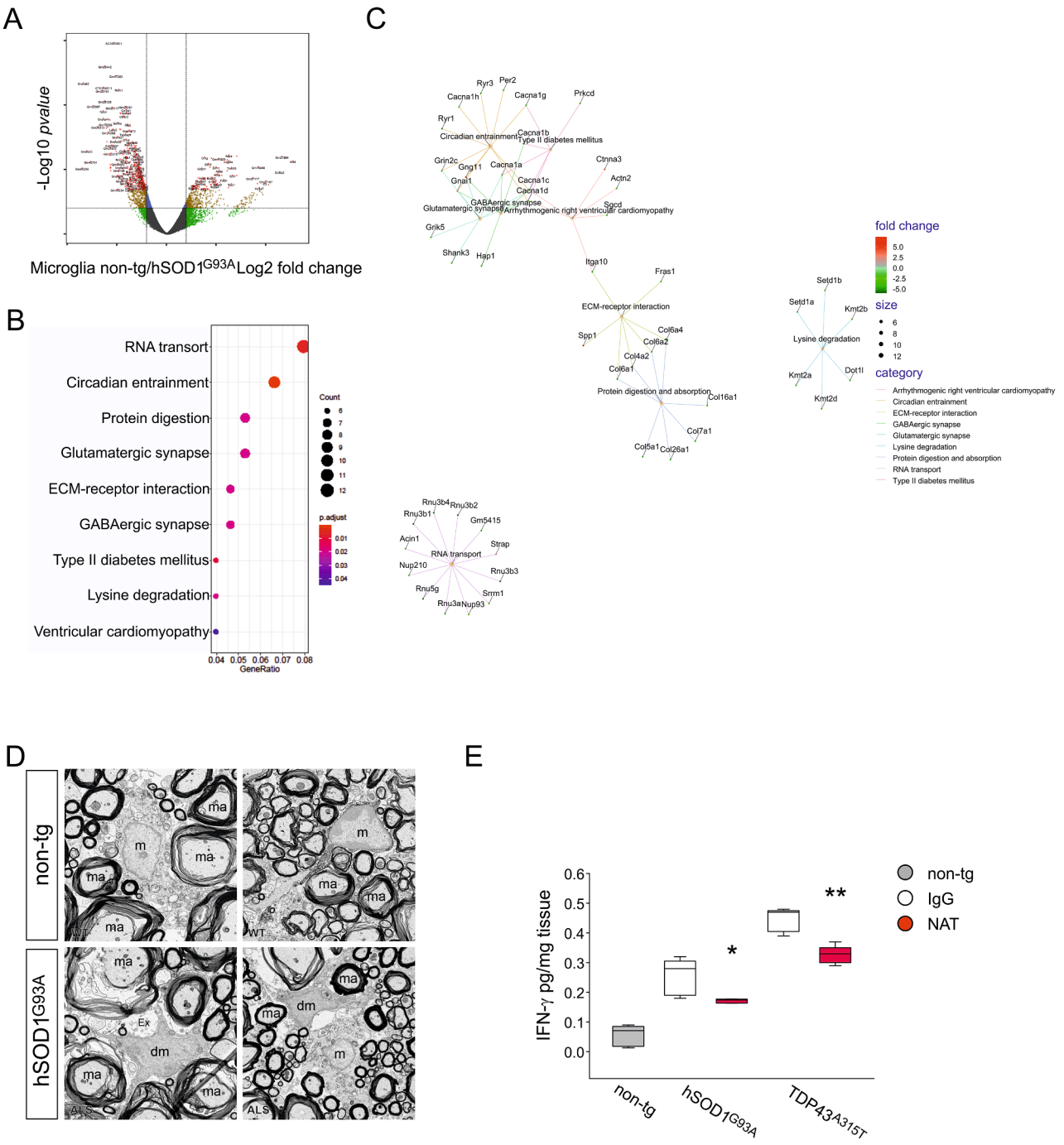


**Fig. 2.** RNA-seq and dark microglia analysis in the spinal cord of hSOD1$^{G93A}$ mice. A) Comparison of gene expression profiles resulting from hSOD1$^{G93A}$ (n = 4) compared to non-tg microglia (n = 4). Each point on the scatterplot represents one gene. The X-axis shows expression ratio (non-tg/ hSOD1$^{G93A}$ microglia) on the log2 scale. Y-axis presents corresponding p-values (–log10[p-value]). Genes that are significantly upregulated in hSOD1$^{G93A}$ microglia (*t*-test p-value < 0.05, fold-change > 4) are marked by colored dots. B) Results of Gene Ontology over-representation analysis (Bonferroni corrected p-values < 0.05) of the genes that are upregulated in microglia sorted from the lumbar spinal cord of hSOD1$^{G93A}$ mice (16 weeks old). C) Network analysis of the hSOD1$^{G93A}$ microglia underlying the genes directly or indirectly interacting with several pathway. D) Scanning electron microscopy showing abundant dark microglia (dm) interacting with myelinated axons (ma) and typical microglia (m) in the spinal cord ventral horn of hSOD1$^{G93A}$ mice compared to non-tg wild-type (WT) controls. E) Expression of IFN-γ in the spinal cord of non-tg, hSOD1$^{G93A}$ and TDP43$^{A315T}$ mice (13 weeks old) treated with control IgG or NAT (n = 5, **P < 0.001 one-way ANOVA). For boxplots the center line, boxes and whiskers represent the median, inner quartiles, and rest of the data distribution, respectively.

to shaping the microglial phenotype in ALS models, we first investigated if the blockade of immune cell infiltration could reduce IFN- γ levels and affect microglial state. Preliminarily, we tested the effect of NAT treatment on the infiltration of (CD45$^{high}$ cells) in the spinal cord (5 weeks of treatment), and data presented in Fig. S1A confirm the efficacy of NAT treatment in hSOD1$^{G93A}$ mice. Fig. 2E shows that in the lumbar spinal cord of NAT-treated mice, IFN-γ level was significantly reduced compared to vehicle-treated hSOD1$^{G93A}$ mice (13 weeks of age), as well as in TDP43$^{A315T}$ mice (10 weeks), since the early-symptomatic stage.

Afterwards, microglial cells were isolated from the lumbar spinal cord of hSOD1$^{G93A}$ mice (16 weeks) treated with NAT or vehicle for 8 weeks, and RNA-seq was performed, focusing on pathways related to

pro-, anti-inflammatory and neurodegenerative genes. Analysis of RNA-seq revealed differences between vehicle and NAT treated hSOD1$^{G93A}$ microglia in various pathways (Fig. 3A–D). Notably, NAT treatment modified the microglial expression of pro-inflammatory and neurodegenerative genes, as well as of genes involved in the regulation of actin cytoskeleton (Fig. 3C, D), showing a transcriptomic profile more similar to non-tg microglia (Fig. S2A). We previously demonstrated that the absence of NK cells shaped the microglial expression of pro- *(il-6, il-1 β tnf- α* and *nos2)* and anti- (*chil3*, *arg-1*, *socs3* and *bdnf)* inflammatory genes in hSOD1$^{G93A}$ mice (Garofalo et al., 2020). To investigate the effect of the non-specific blockade of immune cell infiltration on the expression of these genes in microglia, we performed qPCR analyses: NAT treatment abolished the increased expression of *il-6, il-1β* and *tnf-α*, but further increased *nos2* (Fig. 3F), as well as *chil3* and *arg-1* expression, while *socs3* and *bdnf* were reduced (Fig. 3G). These data suggest that NAT treatment induces a less pronounced reduction of inflammation in comparison with the selective NK cell depletion (Garofalo et al., 2020) and a more complex scenario, likely due to the unspecific blockade of peripheral immune cells infiltration in the CNS.

Since microglial cell morphology is modified in different activation states, we then investigated the effect of NAT treatment on microglial cell morphology in hSOD1$^{G93A}$ mice. Using microscopy, we analyzed ionized calcium-binding adapter molecule 1 (Iba1) (a widely used microglia/macrophages marker) positive cells in the ventral horn of the spinal cord after NAT treatment, measuring the complexity of cell branching and total area covered by the cells. The results obtained showed that NAT treatment of hSOD1$^{G93A}$ mice reduced microglial soma area while increased branch length and their competence area, compared to vehicle-treated mice (Fig. 4A). Furthermore, the blockade of immune cell extravasation reduced the number of Iba1$^{+}$ cells within the spinal cord (Fig. 4B); this could be explained with an effect on macrophage infiltration and/or on microglial proliferation, also considering the reduction of CD45$^{low}$ cells (Fig. S1A).

### 2.3. VLA-4 blockade modifies the transcriptomic profile of astrocytes in the lumbar spinal cord.

Astrocytes are key players in the neurodegenerative and inflammatory events taking place in ALS (Peric et al., 2017; Haidet-Phillips et al., 2011; Gong et al., 2000), and dynamically communicate with immune cells to drive the inflammatory response in the microenvironment (Vahsen et al., 2021; Beers and Appel, 2019). Here, we performed RNA-seq on astrocytes freshly-isolated from the lumbar spinal cord of non-tg, vehicle or NAT-treated hSOD1$^{G93A}$ mice (16 weeks old), to investigate their gene-expression profiles. Unbiased evaluation of translated RNA-seq data demonstrated a significant astrocytic diversity in the absence of infiltrated immune cells: the number of common genes in non-tg and NAT-treated SOD1 astrocytes (93 genes) was higher that non tg and untreated SOD1 astrocytes (9 genes), suggesting the induction of a more homeostatic phenotype upon NAT treatment (Fig. 5A). Bioinformatics analyses revealed that the modulated genes in astrocytes were associated with the inflammatory response, synaptic transmission, and cell metabolism (Fig. 5B–D). Our results showed that a set of pro-inflammatory and neurodegenerative genes in hSOD1$^{G93A}$ astrocytes exhibit consistent downregulation in the absence of peripheral infiltration (Fig. 5E), while most anti-inflammatory genes were highly expressed in NAT-treated mice (Fig. 5E).

Notably, even if the absence of infiltrating peripheral cells modified the astrocyte gene expression, the number of reactive GFAP$^{+}$ astrocyte in the lumbar spinal cord did not change (Fig. 5F), indicating that GFAP expression does not characterize only inflammatory astrocytes (Li et al., 2020; Yang and Wang, 2015).

### 2.4. Blocking immune cell infiltration in the CNS increases survival and reduces motor signs in hSOD1$^{G93A}$ and TDP43$^{A315T}$mice.

To investigate the outcome of infiltrated peripheral immune cells on ALS progression, hSOD1$^{G93A}$ and TDP43$^{A315T}$ mice were treated starting from the pre-symptomatic stage (8 weeks) with NAT as illustrated in Fig. 6A, E, and analyzed for survival time, motor signs onset and progression. Our data demonstrated that NAT treatment increased the survival time and delayed the onset of paralysis in both ALS mouse models (Fig. 6B, C, F). Furthermore, blocking immune cell infiltration delayed the deficits in limb extension reflex, and ameliorated locomotor activity and motor coordination using the inverted grid and Rotarod tests (Fig. 6D, G). No sex-dependent effect of NAT was observed, with similar results obtained with female and male hSOD1$^{G93A}$ mice (Fig. S3A-C). To further evaluate the effect of the peripheral immune cells on ALS progression, we treated hSOD1$^{G93A}$ mice with NAT starting from the early-symptomatic stage (13 weeks), when different immune cell populations (such as NK cells, see Garofalo et al., 2020) already infiltrated the CNS within the ALS affected regions (see scheme in Fig. S3D). Interestingly, also this late NAT administration showed similar effects on mouse survival and motor signs (Fig. S3E–G), suggesting a possible rapid turnover and a continuous entry of immune cells in the CNS during ALS progression. We then investigated whether the effects of NAT on hSOD1$^{G93A}$ mice were accompanied by a reduction of MN degeneration: data shown in Fig. 6H report that NAT treatment increased the number of Smi32$^{+}$ cells (similar results were obtained analyzing Chat$^{+}$ cells, see Fig. S3H) in the lumbar spinal cord of hSOD1$^{G93A}$ mice (16 weeks), demonstrating a protective effect of the CNS microenvironment on MN degeneration, which represents the main hallmark of ALS pathology.

## 3. Discussion

It is now widely accepted that ALS is a non-cell autonomous disease and that motor neuron death is not independent of alteration of the local microenvironment (Liu and Wang, 2017; Vahsen et al., 2021). Several recent studies demonstrated that inflammation is part of the neurodegenerative processes taking place in ALS, while microglial cell reactivity and astrogliosis, accompanied by the expression of pro-inflammatory genes, such as *Il-1b*, *Tnf-α* and *Inos*, are common elements in patients and in experimental models of the disease (Parisi et al., 2013; McGeer and McGeer, 2002; Clarke and Patani, 2020; Peric et al., 2017; Chiu et al., 2013; Cocozza et al., 2018).

In this scenario, peripheral immune cells infiltrate the CNS in ALS affected regions, both in the brain and spinal cord: a longitudinal cohort study of blood from sALS and fALS patients revealed an increased number of circulating T and NK cells (Murdock et al., 2017), and a higher level of immune cell infiltration, at late disease stage, in the spinal cord of hSOD1$^{G93A}$ mice (Finkelstein et al., 2011). Nevertheless, the balance between the protective and detrimental role of infiltrating immune cells in ALS remains largely undetermined, possibly due to the different functions of the immune cell subsets, the region of cell infiltration and the stage of the pathology. It has been demonstrated that the T regulatory (Treg) cells infiltrate the CNS (Garofalo et al., 2020) and are underrepresented in the blood of hSOD1$^{G93A}$ mice (Beers, 2011). These findings suggested that Treg administration might be useful to delay the disease progression and to increase survival (Henkel et al., 2013). Nevertheless, other immune cell subsets were shown to have a detrimental role in the CNS, supporting neurodegeneration and inflammation. We have previously demonstrated that, in mouse ALS models, NK cells can directly kill MNs and switch microglial cells toward a pro-inflammatory phenotype (Garofalo et al., 2020). Activated SOD1-mutant CD8$^{+}$ T cells produce IFN-γ, which elicits the expression of the MHC-I complex in MNs and mediates their cytotoxic function through the Fas and granzyme pathways (Unger et al., 2020). Moreover, infiltrated peripheral macrophages, in ALS affected regions, drive microglia

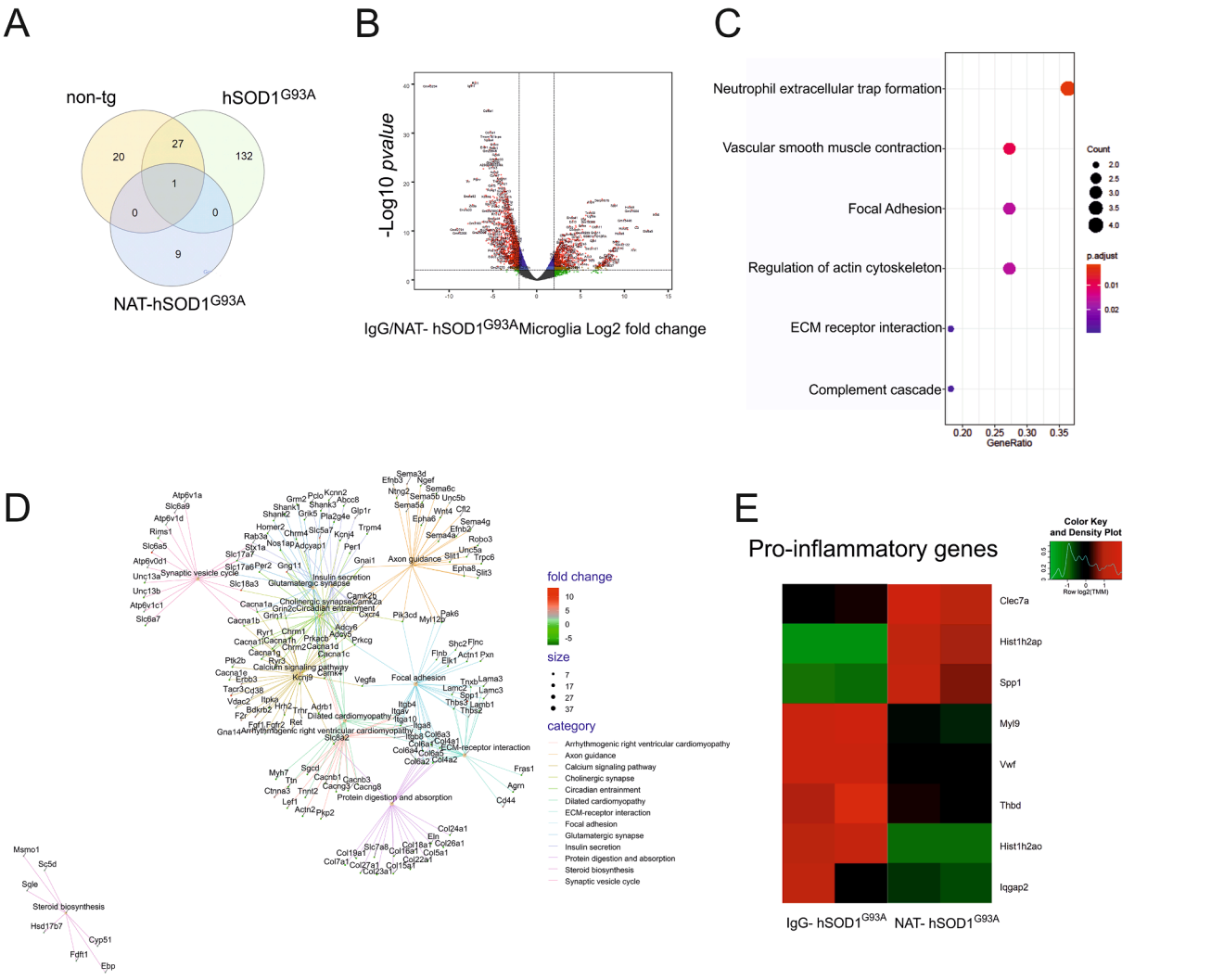


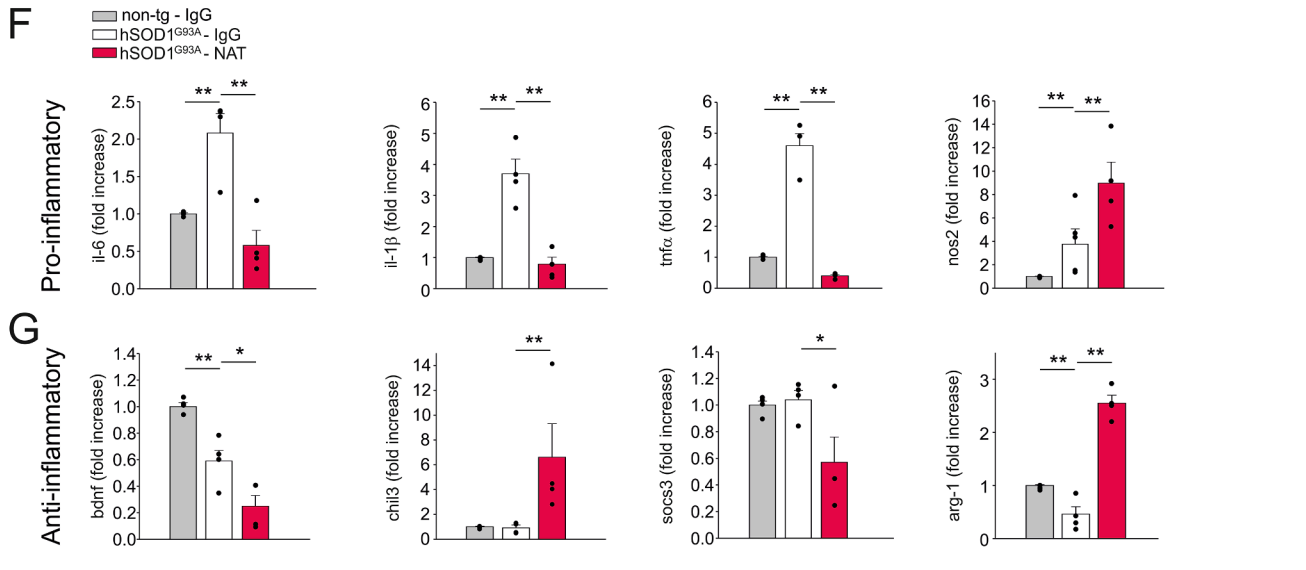


*(caption on next page)*

**Fig. 3.** NAT modulates microglial gene expression in the lumbar spinal cord of hSOD1$^{G93A}$ mice. A) Differential gene expression between non-tg and IgG/NAT-hSOD1$^{G93A}$ microglia collected from the lumbar spinal cord of mice. B) Comparison of gene expression profiles resulting from NAT-hSOD1$^{G93A}$ (n = 4) compared to IgG-hSOD1$^{G93A}$ microglia (n = 4). Each point on the scatterplot represents one gene. The X-axis shows expression ratio (NAT/IgG- hSOD1$^{G93A}$ microglia) on the log2 scale. Y-axis presents corresponding p-values (–log10[p-value]). Genes that are significantly upregulated in NAT-hSOD1$^{G93A}$ microglia (*t*-test p-value < 0.05, fold-change > 4) are marked by colored dots. C) Network analysis of the NAT-hSOD1$^{G93A}$ microglia underlying the genes directly or indirectly interacting with several pathway. D) Results of Gene Ontology over-representation analysis (Bonferroni corrected p-values < 0.05) of the genes that are upregulated in microglia sorted from the lumbar spinal cord of NAT treated hSOD1$^{G93A}$ mice (16 weeks old). E) Expression profile of genes associated with immune response according to the Gene Ontology database and manually selected pro-inflammatory genes. F,G) Gene expression of pro- (F) and anti-inflammatory (G) genes in microglia isolated from the lumbar spinal cord of non-tg or hSOD1$^{G93A}$ mice treated with IgG or NAT. Each dot represents one mouse (n = 4. Data are the mean ± S.E.M. * P < 0.05 ** P < 0.01 one-way ANOVA).

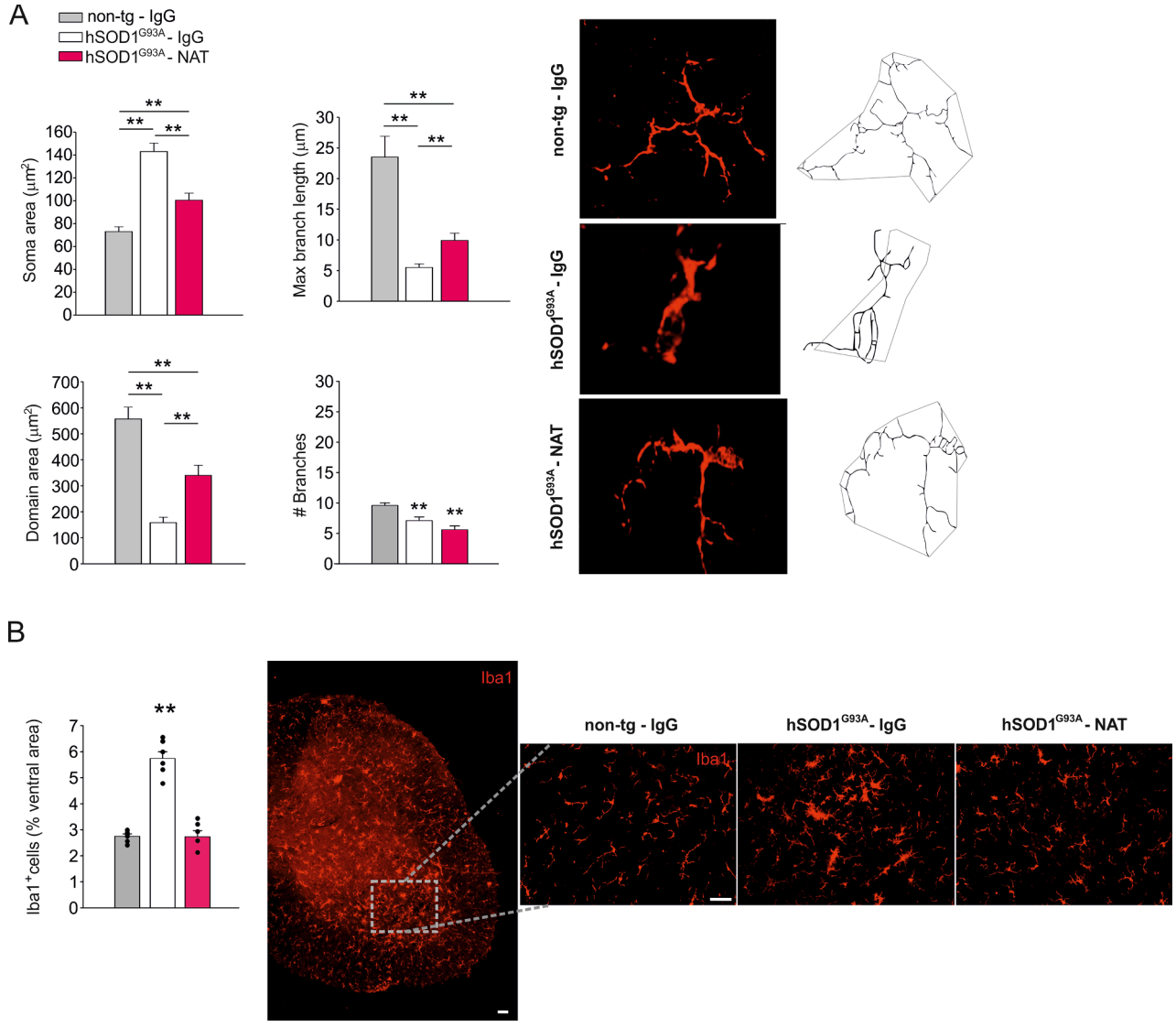


**Fig. 4.** NAT treatment shapes microglial morphology in hSOD1$^{G93A}$ mice. A) Quantification of soma area, scanning domain and branch length of Iba1$^{+}$ cells in slices obtained from the spinal cord of non-tg and hSOD1$^{G93A}$ mice treated with IgG or NAT (n = 4 mice per treatment, 30 cells per mice in at least 6 slices. ** P < 0.01 one-way ANOVA). B) Mean (±S.E.M.) area of Iba1$^{+}$ cells (expressed as % of spinal cord area) in non-tg or hSOD1$^{G93A}$ mice (16 weeks old) treated with IgG or NAT. Each dot represents one mouse (n = 6, ** P < 0.01 one-way ANOVA). Right: representative immunofluorescence image of Iba1$^{+}$ cells in the ventral horn of spinal cord sections. Scale bar: 50 µm.

toward a pro-inflammatory state from an early symptomatic stage (Chiot et al., 2020). Here, we report the presence of CD3$^{+}$ T cells in the spinal cord of sALS patients, and we describe that CD8$^{+}$ T cells directly and specifically contact MNs in the ventral horn, suggesting a possible cytotoxic function, as seen in ALS mouse models (Garofalo et al., 2020; Coque et al., 2019). It must also be considered that CD8$^{+}$ T lymphocytes could exert peripheral neuroprotective activity while resulting toxic for motor neuron soma (Nardo et al., 2018), adding further complexity levels. The role of CD4$^{+}$ T lymphocytes infiltrating the spinal cord in ALS is also controversial: they could contribute to neurodegeneration (Gate et al., 2021) or represent a failed attempt to promote motor neuron protection (Jones et al., 2015), and further experiments will be necessary to better clarify this aspect.

The observation that damage to the blood–brain and blood–spinal cord barriers contribute to early MN degeneration in ALS patients and mice, while restoration of barrier integrity delays the onset of

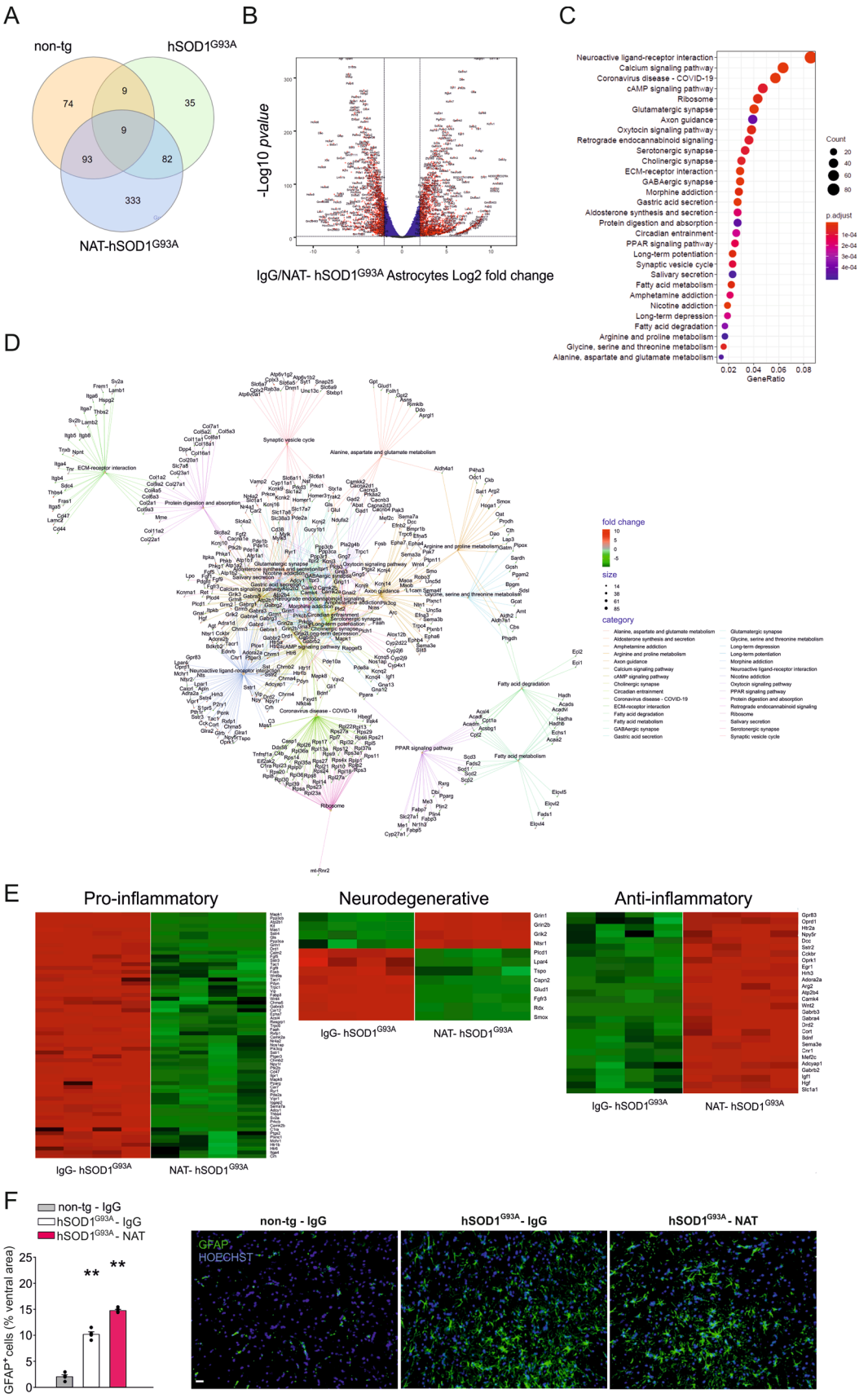


*(caption on next page)*

**Fig. 5.** The blockade of immune cell infiltration affects astrocytic phenotype in the spinal cord of hSOD1$^{G93A}$ mice. A) Differential gene expression between non-tg and IgG/NAT- hSOD1$^{G93A}$ astrocytes collected from the lumbar spinal cord of mice. B) Comparison of gene expression profiles resulting from NAT-hSOD1$^{G93A}$ (n = 4) compared to IgG-hSOD1$^{G93A}$ astrocytes (n = 4). Each point on the scatterplot represents one gene. The X-axis shows expression ratio (NAT/IgG- hSOD1$^{G93A}$ astrocytes) on the log2 scale. Y-axis presents corresponding p-values (–log10[p-value]). Genes that are significantly upregulated in NAT-hSOD1$^{G93A}$ astrocytes (*t*-test p-value < 0.05, fold-change > 4) are marked by colored dots. C) Results of Gene Ontology over-representation analysis (Bonferroni corrected p-values < 0.05) of the genes that are upregulated in astrocytes sorted from the lumbar spinal cord of NAT treated hSOD1$^{G93A}$ mice (16 weeks old). D) Network analysis of the NAT-hSOD1$^{G93A}$ astrocytes underlying the genes directly or indirectly interacting with several pathway. E) Expression profile of genes associated with immune response according to the Gene Ontology database and manually selected pro- and anti-inflammatory and neurodegenerative genes. F) Mean (±S.E.M.) area of GFAP$^+$ cells (expressed as % of spinal cord area) in non-tg or hSOD1$^{G93A}$ mice (16 weeks old) treated with IgG or NAT. Each dot represents one mouse (n = 4 mice per treatment). Right: representative immunofluorescence image of GFAP$^+$ cells in spinal cord sections. Scale bar: 50 μm.

neurodegeneration and disease progression (Liu and Wang, 2017), supports the net positive effect of reducing immune cell infiltration in this pathology. In several neurodegenerative diseases, peripheral immune cells infiltrate the CNS and enhance inflammation releasing pro-inflammatory cytokines that support a toxic activity of glial cells toward neurons (Unger et al., 2020; Earls and Lee, 2020; Hemmer et al., 2015; Stephenson et al., 2018). However, the relationships between immune and glial cells are not linear, being affected by different variables, such as the phenotype and the distribution of reactive astrocytes and microglia, the previous history of these cells, and the stage of the disease (Stephenson et al., 2018).

In the current study, we investigated the mechanisms underlying the immune cell-glial cell communication in two different fALS mouse models, hSOD1$^{G93A}$ and TDP43$^{A315T}$, both characterized by inflammation and immune cell infiltration in the CNS (McGeer and McGeer, 2002; Wegorzewska et al., 2009). It is reported that TDP43$^{A315T}$ mice suffer from intestinal dysmotility due to the degeneration of NOS neurons in the myenteric plexus (Herdewyn et al., 2014; Hatzipetros et al., 2014). Nevertheless, these mice exhibit glial cell reactivity, CNS inflammation, and lymphocyte infiltration during ALS pathological progression (Garofalo et al., 2020; Spiller et al., 2018; Zamudio et al., 2020), representing an acceptable additional model for studying the effects of NAT treatment on ALS progression.

Our results indicated that NAT treatment efficiently reduces the number of infiltrated leukocytes and modulates the expression of genes related to inflammation and neurodegeneration both in microglial cells and astrocytes. Bioinformatics analyses revealed that in microglia the downregulated genes were mainly associated with the inflammatory response and the regulation of the actin cytoskeleton. Consistently, in the lumbar spinal cord of hSOD1$^{G93A}$ mice, NAT-treatment affected microglial morphology, reducing soma area, increasing the length of their branches, which covered a wider parenchymal area. This result may be explained with a direct modulation of microglial genes involved in cell cytoskeleton remodelling, and to the re-acquisition of a surveillant phenotype, as also suggested by the increased mRNA expression of anti-inflammatory genes. Additional experiments would be necessary to better address the effects of NAT treatment on proteins involved in determining the inflammatory and anti-inflammatory microglial phenotype.

In astrocytes, the transcriptomic analyses revealed that NAT treatment affects pathways involved in different cellular functions, such as inflammation, synaptic transmission or elimination, cell metabolism, neuronal plasticity, and synaptic vesicle cycle, suggesting a strong connection of astrocytes with the infiltrating immune cells in ALS that will deserve further investigation. In several neurodegenerative diseases, astrocytes can sense and respond to various inflammatory signals secreted by infiltrating lymphocytes, resulting in the production of chemokines that ultimately lead to chronic CNS inflammation and neurodegeneration (Linnerbauer et al., 2020). Moreover, bidirectional interactions with astrocytes actively shape the recruitment, diapedesis, and extravasation of leukocytes (Linnerbauer et al., 2020). Here we suggest that this crosstalk could drive the detrimental response during ALS progression, modifying the astrocytic phenotype, that is re-directed toward a homeostatic gene expression by NAT treatment.

We hypothesized that the modulation of glial gene expression induced by NAT treatment is related with the reduced level of cytokines produced by infiltrating leukocytes, such as IFNγ. The main source of IFN-γ in the ALS affected regions are CD8$^+$ T and NK cells (Garofalo et al., 2020; Coque et al., 2019), and their absence could justify the reduction we observed in NAT-treated mice. This hypothesis is further supported by previous data showing that IFN-γ depletion reduced disease progression in ALS models (Garofalo et al., 2020), and that IFN-γ directly modulates the transcriptomic response of astrocytes and microglia, notably of cytokines and chemokines related to the inflammatory response (Rock et al., 2005; Smith et al., 2020). Our result that NAT treatment did not completely abolish the high levels of IFN-γin the spinal cord, in spite of an almost complete elimination of infiltrating leukocytes, opens the possibility to other possible local sources (Mäkelä et al., 2010), or to a peripheral origin due to a compromised blood–brain/spinal barrier (Garbuzova-Davis et al., 2007; Garbuzova-Davis et al., 2012). It must be considered that peripheral immune cells could also affect microglial reactivity, with impact on ALS disease progression (Chiot et al., 2020) and we cannot exclude that part of the effects described with NAT are mediated through peripheral immune cells.

The observation that the blockade of the immune cell infiltration in different disease stages increased mouse survival (both hSOD1$^{G93A}$ and TDP43$^{A315T}$ models) and the number of healthy MNs supports the classification of ALS as a non-cell-autonomous disease, where MN degeneration results from a defective communication with immune and glial cells (Vahsen et al., 2021; McGeer and McGeer, 2002; Boillée et al., 2006).

Altogether, our data highlight the key role of peripheral immune cells in ALS onset and progression, and in the transition to an inflammatory CNS microenvironment. Indeed, the failure of anti-inflammatory and anti-immune therapies in clinical trials highlighted the scarce understanding of the immune changes across the disease course, supporting the need to further investigate the immune response in ALS. The positive effects of NAT on ALS mouse models open to a possible drug repositioning for future clinical trials in patients. Our study suggest that a multi-cellular approach could give better results to counteract disease progression and that targeting the molecular pathways involved in immune cell extravasation in the CNS could be a novel approach to modulate the inflammatory states of microglia and astrocytes, slowing down the neurodegenerative processes in ALS.

## 4. Materials and methods

### 4.1. Materials

The Thermo Script RT-PCR System, secondary Abs, and Hoechst (catalogue #33342, RRID:AB_10626776) were from GIBCO Invitrogen (Carlsbad, CA, USA). Glucose, Percoll, phosphate buffered-saline (PBS) tablet (#P4417), and Bovine Serum Albumin (BSA) were from Sigma-Aldrich (Milan, Italy). Chloral hydrate (#334085) was from Carlo Erba (Milan, Italy). ChAT (#AB144P) Ab was from Merck Millipore (Milan, Italy). IFNγ ELISA kit (KAC1231) was from Life technologies Invitrogen (Carlsbad, CA, USA). Microbeads ACSA+ (#130–097-678) were from Miltenyi Biotec (Bologna, Italy). RNeasy Mini Kit was from Qiagen (Hilden, Germany). CD45, CD3, CD4 and CD8 were from eBioscience Inc., (San Diego, CA). Rabbit anti-Iba1 (Cat# 019–19741, RRID:

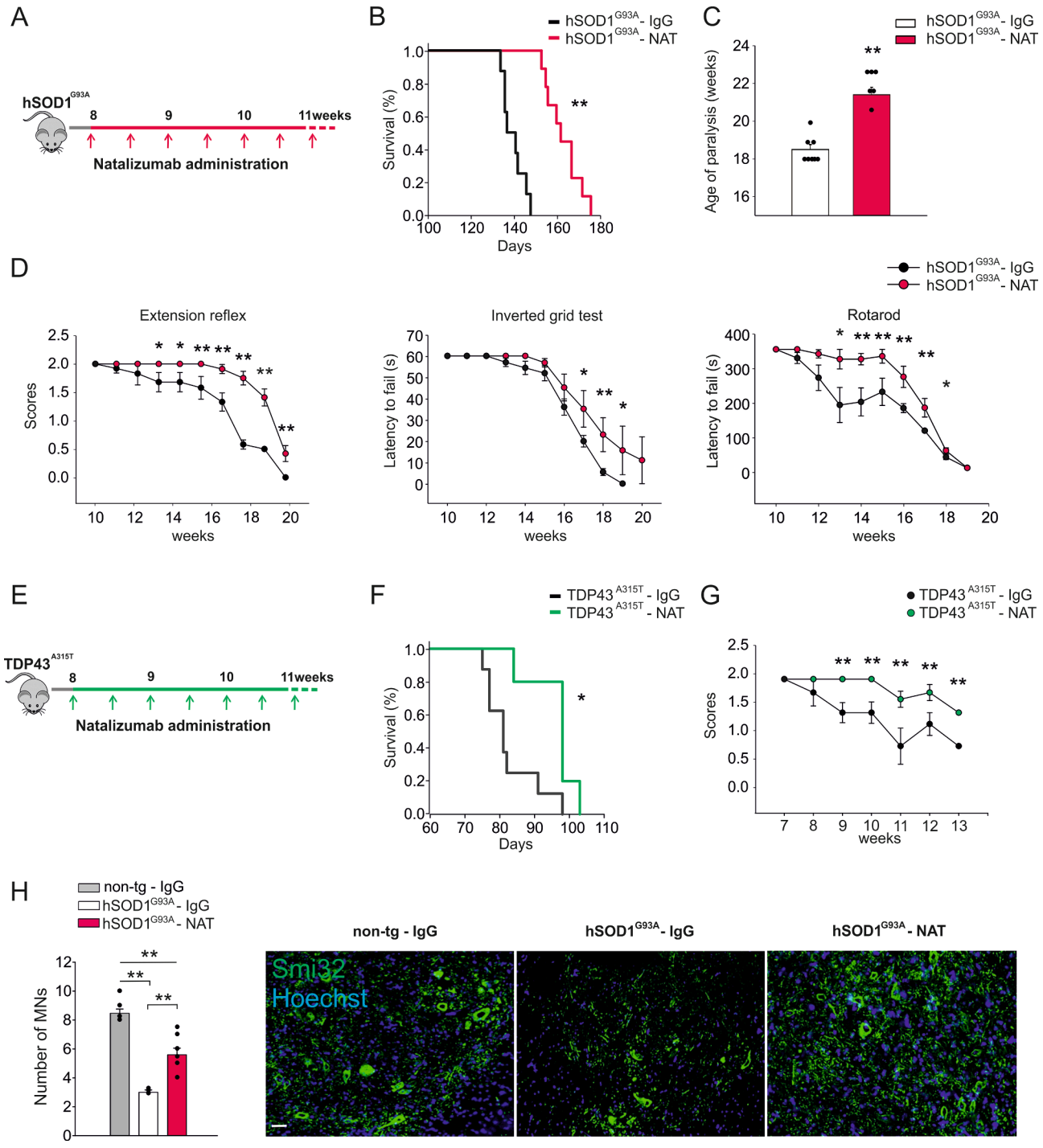


**Fig. 6.** NAT increases survival modulating motor function in hSOD1$^{G93A}$ and TDP43$^{A315T}$ mice. A) Scheme of mice treatment with NAT. B) Kaplan-Meier curve of hSOD1$^{G93A}$ treated with IgG or NAT (n = 9–10, hSOD1$^{G93A}$ IgG: 139.6 ± 1.9 days; NAT: 162.2 ± 2.6 days, data are the mean ± S.E.M. ** $P < 0.01$ log-rank test). C) Age of paralysis of hSOD1$^{G93A}$ mice treated with IgG or NAT. Each dot represents one mouse (n = 9–10, IgG: 18.5 ± 0.3 weeks; NAT: 21.4 ± 0.4 weeks. Data are the mean ± S.E.M. ** $P < 0.01$ Student's *t* Test). D) Analyses of motor function in hSOD1$^{G93A}$ mice treated with NAT or IgG with: extension reflex (left), inverted grid test (center) and rotarod test (right). Behavioral tests were performed once a week, starting from 8 weeks (n = 10 mice per treatment. Data are expressed as mean ± S.E.M. * $P < 0.05$, ** $P < 0.01$ *vs* IgG-treated mice, one-way ANOVA). E) Scheme of mice treatment with NAT, starting from 8 weeks. F) Kaplan-Meier curve of TDP43$^{A315T}$ treated with IgG or NAT (n = 8, TDP43$^{A315T}$ IgG: 89.3 ± 2.4 days; NAT: 95.2 ± 1.6 days, data are the mean ± S.E.M. ** $P < 0.01$ log-rank test). G) Analyses of extension reflex in TDP43$^{A315T}$ mice treated with NAT or IgG performed twice a week, starting from 8 weeks (n = 8 mice per treatment. Data are expressed as mean ± S.E.M. ** $P < 0.01$ *vs* IgG-treated mice, one-way ANOVA). H) Quantification of Smi32$^{+}$ - MNs in the ventral horns of the spinal cord in non-tg and hSOD1$^{G93A}$ mice treated with IgG or NAT (n = 6. Data are shown as mean ± S.E.M. ** $P < 0.01$ one-way ANOVA). Scale bar: 40 μm.

AB_839504) was from Wako (VA, USA). GFAP Ab EPR1034Y (ab68428) was from Abcam (Cambridge, UK). CD31 Ab (#3568 S, RRID: AB_10694616) was from Cell Signaling (WZ Leiden, The Netherlands). SMI-32 Ab was from BioLegend (San Diego, CA). Natalizumab (anti-VLA-4 (CD49d)) (#BE0071, RRID:AB_1107657) was from Bioxcell (West Lebanon, USA). Reagents and consumables for electron microscopy sample processing were from Electron Microscopy Sciences (EMS; Hatfield, PA, USA).

### 4.2. Animals

Experiments described in the present work were approved by the Italian Ministry of Health (authorization n. 78/2017-PR) in accordance with the guidelines on the ethical use of animals from the European Community Council Directive of September 22, 2010 (2010/63/EU), and from the Italian D.Leg 26/2014. All possible efforts were made to minimize animal suffering, and to reduce the number of animals used per condition by calculating the necessary sample size before performing the experiments. Male and female hSOD1G93A [B6.Cg-Tg(SOD1-G93A) 1Gur/J line, the transgene copy number is typically 17–23] (RRID:IMSR_JAX:004435), and TDP43A315T [B6.Cg-Tg(Prnp-TARDBP*A315T)95Balo/J] (Cat# JAX:010700, RRID: IMSR_JAX:010700), transgenic mice were obtained from Jackson Laboratory (Bar Harbor, ME, USA) and from Charles River (Calco, Italy). hSOD1G93A were also maintained as hemizygotes by breeding transgenic males with wild-type C57BL/6 J females from Charles River Laboratories, both maintained on C57BL/6 J genetic background. Age-matched non-transgenic (non-tg) C57BL/6 J mice were always used as controls. Transgenic mice were identified by PCR on DNA obtained from tail biopsies. Briefly, tail tips were digested (overnight, 58 °C) in a buffer containing 100 mM Tris–HCl pH 8, 0.1% SDS 20, 5 mM EDTA pH 8, 200 mM NaCl and 20 mg/ml proteinase K (Ambion-Thermo Fisher, Germany, #2548) and the genomic DNA was amplified with SsoFast Eva Green Supermix (Bio-Rad, California, #172–5201) using the following primers: SOD1 forward 5′-CATCAGCCCTAATCCATCTGA-3′; SOD1 reverse 5′- CGCGACTAACAATCAAAGTGA-3.

Mice were housed in standard breeding cages at a constant temperature (22 ± 1 °C) and relative humidity (50%), with a 12:12 h light:dark cycle (light on 07.00–19.00 h). Food and water were available ad libitum.

### 4.3. Human spinal cord tissues

Postmortem material was obtained at autopsy from 12 ALS patients at the department of (Neuro)Pathology of the Amsterdam UMC, Academic Medical Center, (University of Amsterdam, the Netherlands) (Table S1). All patients fulfilled the diagnostic criteria for ALS (El Escorial criteria Ludolph et al., 2015) as reviewed independently by two neuropathologists. All patients with ALS died from respiratory failure. Control spinal cord tissue was obtained from eight patients who had died from a non-neurological disease. Both ALS and control patients included in the study displayed no signs of infection before death. Informed consent was obtained for the use of brain tissue and for access to medical records for research purposes and approval was obtained from the relevant local ethical committees for medical research. Tissue preparation: paraffin-embedded tissue was sectioned at 6 μm and mounted on pre-coated glass slides (StarFrost, Waldemar Knittel Glasbearbeitungs GmbH, Braunschweig, Germany). Representative sections of all specimens were processed for haematoxylin and eosin, Klüver-Barrera and Nissl stains.

### 4.4. Mice treatment

Starting at 8 or 13 weeks of age, male and female hSOD1$^{G93A}$, TDP43$^{A315T}$ or non-tg C57BL/6 J mice were randomly grouped for the treatments. We used female mice for all the experiments; males were only used to compare with females in the experiments of survival and behavior. Mice were i.p. injected with 62.5 μg (in 100 μl) of NAT, or with the corresponding control IgG, every 4 days until the age described in the text or until sacrifice for the survival analysis experiments. This dosage was already shown to efficiently block lymphocyte infiltration in the mouse CNS (Gan et al., 2012). The number of peripheral immune cell detection in the CNS was monitored by FACS. In detail immune cells from the spinal cord of non-tg or hSOD1$^{G93A}$ mice were enriched by centrifugation on Percoll 40%, washed in PBS and immunostained with fluorochrome-conjugated anti-CD45.2 to identify leukocytes and analyzed by flow cytometry using a FACSCanto II (BD Biosciences). Data,elaborated using FlowJo Version 9.3.2 software (TreeStar), showed a reduction of CD45$^{high}$ cells of ~ 99% (Fig. S1A).

### 4.5. Survival analysis

hSOD1$^{G93A}$ and TDP43$^{A315T}$ mice were treated with NAT or control IgG as described above and were monitored daily. The endpoint was fixed when animals were unable to stand up within 20 s after being placed on either side, or death. The probability of survival was calculated using the Kaplan–Meier method, and statistical analyses were performed using a log-rank test.

### 4.6. Behavioral tests

Behavioral tests started when mice were 8 weeks old. All animals were handled for at least 5 min/day for 2–3 days before starting the experiments. For the hindlimb extension reflex, mice were suspended by the tail, and scored for hindlimb extension reflex deficits. The scores were recorded from 0 to 2 as follows: 2, normal extension reflex in both hind limbs; 1.5, imbalanced extension in the hind limbs; 1.0, extension reflex in only one hindlimb; 0.5, the absence of any hindlimb extension; and 0, total paralysis. For the inverted grid test mice were placed in the center of a wire grid (40 × 60 cm, suspended 50 cm above a cushioned table) and then the grid was inverted (maximum time allowed 60 s). The time spent hanging on to the grid was measured. For the Rotarod test, motor coordination, strength and balance were assessed using a rotarod apparatus (Ugo Basile, Gemonio Italy, #47650). Animals were placed onto the cylinder at a constant speed of 15 rpm. The arbitrary cut-off time was 300 s., and the longest latency was recorded.

### 4.7. Immunostaining and data analysis

In different stages of pathology, mice were overdosed with chloral hydrate (400 mg/kg, i.p.) and then intra-cardially perfused with PBS and then PFA 4%; spinal cord was then isolated, fixed in 4% formaldehyde and snap frozen. Cryostat sections (20 μm) were washed in PBS, blocked (3% goat serum in 0.3% Triton X-100) for 1 h, at RT, and incubated overnight at 4 °C with specific antibodies diluted in PBS containing 1% goat serum and 0.1% Triton X-100. The sections were incubated with the following primary Abs: anti-Smi32 (1:500), anti-ChAT (1:100), anti-Iba1 (1:500) and anti-GFAP (1:1000). For immunostaining on paraffin embedded human spinal cord section, tissues were placed at 60 °C for 15 min, incubated in xylene at RT for 25 min, and then transferred sequentially into 100% EtOH, 95% EtOH, 70% EtOH, and 50% EtOH for 4 min at RT. The sections were rinsed in deionized water and incubated with Abs: anti-Smi32 (1:500), anti-CD31, CD3, CD4, CD8 (1:200). After several washes, sections were stained with the fluorophore-conjugated antibody and Hoechst for nuclei visualization and analyzed using a fluorescence microscope. For co-immunofluorescence, the secondary antibody was subsequently used. For Iba1 and Smi32 staining, antigen retrieval was performed and the coronal sections were first boiled for 20 min in citrate buffer (pH 6.0) at 95–100 °C. For Iba1 and GFAP analysis, Images were digitized using a CoolSNAP camera (Photometrics) coupled to an ECLIPSE Ti-S microscope (Nikon) and processed using MetaMorph 7.6.5.0 image analysis

software (Molecular Device). Slices were scanned by consecutive fields of vision (×10 objective lens) to build a single image per section. Data were expressed as area occupied by fluorescent cells versus total area by converting pixel to mm. For comparison between different treatments, at least 12 coronal sections per lumbar spinal cord were analyzed.

### 4.8. Motor neuron survival evaluation

For MN survival, the whole ventral horns of lumbar spinal cord were photographed at × 20 magnification and digitized using a CoolSNAP camera (Photometrics) coupled to an ECLIPSE Ti-S microscope (Nikon) and processed using MetaMorph 7.6.5.0 image analysis software (Molecular Device). The number of MNs was evaluated counting only Smi32- or ChAT-positive cells with typical morphology triangular shape, single well-defined axon, large body diameter (≥20 μm) and intact axons and dendrites. This analysis was done in at least 12 serial slices for each animal.

### 4.9. Electron microscopy (EM)

Mice were anesthetized with chloral hydrate (400 mg/kg, i.p.) and then intra-cardially perfused with 250 ml of 0.1% glutaraldehyde in PFA 4%. Coronal sections of the spinal cord were selected. Sections from 3 hSOD1$^{G93A}$ and 3 age-matched non-tg controls were post-fixed flat in 2% osmium tetroxide and 1.5% potassium ferrocyanide for 1 h, followed by incubation in 1% thiocarbohydrazide for 20 min, and further incubated in 2% osmium tetroxide as described by the National Center for Microscopy and Imaging Research (Savage et al., 2020). Following post-fixation, sections were dehydrated in increasing concentrations of ethanol and immersed in propylene oxide. Following dehydration, sections were impregnated with Durcupan resin (Electron Microscopy Sciences; EMS) overnight at room temperature, mounted between ACLAR embedding films (EMS) and cured at 55 °C for 72 h. Specific regions of interest from the ventral horn of lumbar spinal cord were excised and mounted on resin blocks for ultrathin sectioning (52). Ultrathin sections (~75 nm thickness) were collected and placed on a silicon nitride chip and glued onto specimen mounts for scanning electron microscopy (SEM). Imaging was conducted at 5 nm of resolution using a Crossbeam 540 field emission SEM with a Gemini column (Zeiss).

### 4.10. Isolation of lumbar microglial cells

Adult microglia were isolated from the lumbar spinal cord tract of age-matched non-tg C57BL/6 J mice and hSOD1$^{G93A}$ mice as in (Cocozza et al., 2018). In detail, mice were deeply anesthetized with chloral hydrate (i.p., 400 mg/Kg) before being transcardially perfused with PBS. Spinal cords were then flushed out from the spinal canal using a 20 ml syringe filled with PBS and digested with 30 units of papain (15–23 U/mg protein) for 30 min at 37 °C with continuous rocking to ensure tissue sections were suspended. After allowing the tissue sections to settle for 5 min, the media was discarded and 2 ml of DMEM + GlutaMax-1 media (Gibco) supplemented with 15% heat inactivated fetal bovine serum (Gibco) and 1% Penicillin-Streptomycin (Gibco) was added. Tissue was then triturated with a pipette to obtain single-cell suspensions, which were applied to 70 μm/40 μm cell strainers and used for the experiments. The cell suspension in a final volume of 6 ml media was centrifuged at 397 × g for 5 min at room temperature before the supernatant was discarded and the pellet suspended in fresh 1 ml media. Purity of isolated microglia cells is assessed by FACS and ranges between 70 and 90%, and were selected only the samples in which the purity was 90%. Total RNA was isolated with RNeasy Mini Kit, and processed for real-time PCR and RNA-seq. The quality and yield of RNAs were verified using the NANODROP One system (Thermo Scientific).

### 4.11. Isolation of lumbar astrocytes

Adult astrocytes were isolated from the lumbar spinal cord tract of age-matched non-tg C57BL/6 J mice and hSOD1$^{G93A}$ mice. Spinal cord was removed, tissues were cut into small pieces and single-cell suspension was achieved in Hank's balanced salt solution (HBSS). The tissue was further mechanically dissociated using a glass wide-tipped pipette and the suspension was applied to a 30 μm cell strainer (Miltenyi Biotec). Cells were processed immediately for MACS MicroBead separation. ACSA$^{+}$ cells were magnetically labelled with ACSA MicroBeads. The cell suspension was loaded onto a MACS Column placed in the magnetic field of a MACS Separator and the negative fraction was collected. After removing the magnetic field, ACSA + cells were eluted as a positive fraction, and the purity was > 95%. Live astrocytes were assessed by immunofluorescence and flow cytometry (FACS). After sorting the positive fractions, total RNA was isolated with RNeasy Mini Kit, and processed for real-time PCR and RNA-seq. The quality and yield of RNAs were verified using the NANODROP One system (Thermo Scientific).

### 4.12. Real-time PCR

Microglia and astrocytes were sorted from spinal cord of mice were lysed in Trizol reagent for isolation of RNA. Reverse transcription reaction was performed in a thermocycler (MJ Mini Personal Thermal Cycler; Biorad) using IScript TM Reverse Transcription Supermix (Biorad), under the following conditions: incubation at 25 °C for 5 min, reverse transcription at 42 °C for 30 min, inactivation at 85 °C for 5 min. Real-time PCR (RT-PCR) was carried out in a I-Cycler IQ Multicolor RT-PCR Detection System (Biorad) using SsoFast EvaGreen Supermix (Biorad) according to the manufacturer's instructions. The PCR protocol consisted of 40 cycles of denaturation at 95 °C for 30 s and annealing/extension at 60 °C for 30 s. For quantification analysis, the comparative Threshold Cycle (Ct) method was used. The Ct values from each gene were normalized to the Ct value of GAPDH in the same RNA samples. Relative quantification was performed using the $2^{\Delta DDC}$t method and expressed as fold change in arbitrary values. The primers used were listed in Table S2.

### 4.13. RNA-seq

Microglia and astrocytes were sorted from the lumbar spinal cord tract of age-matched non-tg C57BL/6 J mice and hSOD1$^{G93A}$ mice as reported above. RNA-seq analyses were performed by Bio-Fab research, Italy, Rome. FastQC was used to do some quality control checks on raw untrimmed and trimmed read data from high throughput sequencing (NovaSeq 6000 System, 2 × 150 PE read) before performing any further analysis. The raw read was trimmed (Trimmomatic Version 0.38) by sliding window size and quality threshold, with 4-base wide window and average Phred quality score of 20, respectively. Star alignment program in RSEM package v1.3.3 was used for aligning sequencing PE reads to Ensemble Mouse GRCm39 genome primary assembly. The estimate read count matrix was utilized by EBSeq in RSEM package for downstream differential expression analysis. The EBSeq output was plotted as Volcano Plot.

The genes differentially expressed with Log FC > |2.0| and FDR < 0.05 were selected to generate the pathway analysis by Over-Representation Analysis (ORA). Heatmap Plot was generated from statistically significant pathway observed in at least one group. Plots were created using the ggplot2, a R package dedicated to data visualization.

### 4.14. Morphological analysis of Iba1$^{+}$ cells

Lumbar spinal cord slices from perfused mice were analyzed by confocal microscopy and skeleton analysis to assess Iba1$^{+}$ cell morphology (30 cells per mouse). Twenty mm z-stacks were acquired at 0.5 μm intervals using an FV1000 laser scanning microscope (Olympus)

at × 60 objective. Maximal intensity projections of each image were generated, binarized, and skeletonized using the Skeletonize 2D/3D plugin in ImageJ, after which the Analyze Skeleton plugin (https://imagej.net/AnalyzeSkeleton) was applied. The average branch number (process end points per cell) and length per cell were recorded for each image with a voxel size exclusion limit of 150 applied. The number of single and multiple junction points was additionally calculated to give an indication of branching complexity. The areas of the soma and scanning domain were measured for each cell.

### 4.15. Measurement of IFN-γ by ELISA

The spinal cord of 13-weeks-non-tg, hSOD1$^{G93A}$ and TDP43$^{A315T}$ mice were disrupted with a homogenizer and analyzed for IFN-γ content using a sandwich ELISA, following the manufacturer's instructions (CAT#KAC1231 Life technologies, Invitrogen). Briefly, 96-well ELISA microplates were coated with anti-IFN-γ monoclonal Ab. Samples or IFN-γ standard were added at the appropriate dilution and incubated for 2 h at room temperature. After careful washing, biotinylated goat anti-IFN-γ was added to each well; horseradish-peroxidase was used as secondary Ab and optical density was read at 450 nm.

### 4.16. Statistical analyses

Data are shown as the mean ± S.E.M. Statistical significance was assessed by Student's *t*-test, one-way ANOVA or two-way ANOVA for parametrical data, as indicated; Holm–Sidak test was used as a post-hoc test; Mann–Whitney Rank test and Kruskal–Wallis for non-parametrical data, followed by Dunn's or Tukey's post-hoc tests. For multiple comparisons, multiplicity adjusted p-values are indicated in the corresponding figures (*$p < 0.05$, **$p < 0.01$). For the Kaplan–Meier analysis of survival, the log-rank test was used. Statistical analyses comprising calculation of degrees of freedom were done using Sigma Plot 11.0 and Origin 7. For each experiment, the sample size (n) was chosen considering the following relation: $n \geq 2$sigma (Zalpha/D)2, where sigma is substituted by an estimate of variance (s2); alpha is at 0.05 (and Zalpha = -2) and D is the difference among treatments. Criteria of animal exclusion/inclusion were pre-established; animals considered for the analysis were selected for age. At weaning, pups from different colonies were mixed together and mice were randomly treated. The investigators performing the different analyses always received the samples from a third laboratory member, who was not involved in that specific experiment, to ensure blinding to the group allocation.

## Author contributions

S.G.: performed most of the experimental work and wrote the article; G.C.: contributed to many experimental activities for mice manipulation; G.B.: performed FACS analyses; J.S.: performed EM experiments; M.R.: produced and analyzed transgenic mice phenotype; E.A.: provided human tissues; M.E.T.: supervised EM analyses and wrote the paper; R. M.R.: supervised experiments on microglia gene expression; A.S.: supervised experiments on immune cells; C.L.: supervised all the experimental work and wrote the article.

## Funding

This work was supported by AIRC 22,329 2018, ARISLA NKINALS 2019 to S.G.; PRIN 2017 20178L7WRS_001, AIRC 2019: IG-23010 to C. L. M.E.T. is a Tier II Canada Research Chair in *Neurobiology of Aging and Cognition.* ALS Stichting grant "The Dutch ALS Tissue Bank" (A.E.).

## Appendix A. Supplementary data

Supplementary data to this article can be found online at https://doi.org/10.1016/j.bbi.2022.06.004.

## References

Allen, S.P., Hall, B., Woof, R., Francis, L., Gatto, N., Shaw, A.C., Myszczynska, M., Hemingway, J., Coldicott, I., Willcock, A., Job, L., Hughe, R.M., Boschian, C., Bayatti, N., Heath, P.R., Bandmann, O., Mortiboys, H., Ferraiuolo, L., Shaw, P.J., 2019. C9orf72 expansion within astrocytes reduces metabolic flexibility in amyotrophic lateral sclerosis. Brain 142, 3771–3790.

Beers, D.R., 2011. Neuroinflammation modulates distinct regional and temporal clinical responses in ALS mice. Brain Behav. Immun. 25, 1025–1035.

Beers, D.R., Appel, S.H., 2019. Immune dysregulation in amyotrophic lateral sclerosis: mechanisms and emerging therapies. Lancet Neurol. 18 (2), 211–220.

Beers, D.R., Henkel, J.S., Xiao, Q., Zhao, W., Wang, J., Yen, A.A., Siklos, L., McKercher, S. R., Appel, S.H., 2006. Wild-type microglia extend survival in PU.1 knockout mice with familial amyotrophic lateral sclerosis. Proc. Natl. Acad. Sci. U.S.A. 103 (43), 16021–16026.

Béland, L.C., Markovinovic, A., Jakovac, H., De Marchi, F., Bilic, E., Mazzini, L., Kriz, J., Munitic, I., 2020. Immunity in amyotrophic lateral sclerosis: blurred lines between excessive inflammation and inefficient immune responses. Brain Commun. 2, 2: fcaa124.

Bisht, K., Sharma, K.P., Lecours, C., Sánchez, M.G., El Hajj, H., Milior, G., Olmos-Alonso, A., Gómez-Nicola, D., Luheshi, G., Vallières, L., Branchi, I., Maggi, L., Limatola, C., Butovsky, O., Tremblay, M.E., 2016. Dark microglia: a new phenotype predominantly associated with pathological states. Glia 64, 826–839.

Boillée, Séverine, Yamanaka, K., Lobsiger, C.S., Copeland, N.G., Jenkins, N.A., Kassiotis, G., Kollias, G., Cleveland, D.W., 2006. Onset and progression in inherited ALS determined by motor neurons and microglia. Science 312 (5778), 1389–1392.

Chiot, A., Zaïdi, S., Iltis, C., Ribon, M., Berriat, F., Schiaffino, L., Jolly, A., de la Grange, P., Mallat, M., Bohl, D., Millecamps, S., Seilhean, D., Lobsiger, C.S., Boillée, S., 2020. Modifying macrophages at the periphery has the capacity to change microglial reactivity and to extend ALS survival. Nat. Neurosci. 11, 1339–1351.

Chiu, I., Morimoto, E.A., Goodarzi, H., Liao, J., O'Keeffe, S., Phatnani, H., Muratet, M., Carroll, M., Levy, S., Tavazoie, S., Myers, R., Maniatis, T., 2013. A neurodegeneration-specific gene-expression signature of acutely isolated microglia from an amyotrophic lateral sclerosis mouse model. Cell Rep. 4 (2), 385–401.

Clarke, B.E., Patani, R., 2020. The microglial component of amyotrophic lateral sclerosis. Brain 12, 3526–3539.

Cocozza, G., di Castro, M.A., Carbonari, L., Grimaldi, A., Antonangeli, F., Garofalo, S., Porzia, A., Madonna, M., Mainiero, F., Santoni, A., Grassi, F., Wulff, H., D'Alessandro, G., Limatola, C., 2018. $Ca^{2+}$-activated $K^+$ channels modulate microglia affecting motor neuron survival in hSOD1$^{G93A}$ mice. Brain Behav. Immun. 73, 584–595.

Cocozza, G., Garofalo, S., Morotti, M., Chece, G., Grimaldi, A., Lecce, M., Scavizzi, F., Menghini, R., Casagrande, V., Federici, M., Raspa, M., Wulff, H., Limatola, C., 2021. The feeding behaviour of Amyotrophic Lateral Sclerosis mouse models is modulated by the $Ca^{2+}$ -activated $K_{Ca}$ 3.1 channels. Br. J. Pharmacol. 178 (24), 4891–4906. https://doi.org/10.1111/bph.15665.

Coque, E., Salsac, C., Espinosa-Carrasco, G., Varga, B., Degauque, N., Cadoux, M., Crabé, R., Virenque, A., Soulard, C., Fierle, J.K., Brodovitch, A., Libralato, M., Végh, A.G., Venteo, S., Scamps, F., Boucraut, J., Laplaud, D., Hernandez, J., Gergely, C., Vincent, T., Raoul, C., 2019. Cytotoxic $CD8^+$ T lymphocytes expressing ALS-causing SOD1 mutant selectively trigger death of spinal motoneurons. Proc. Natl. Acad. Sci. U.S.A. 116, 2312–2317.

Earls, R.H., Lee, J.K., 2020. The role of natural killer cells in Parkinson's disease. Exp. Mol. Med. 52 (9), 1517–1525.

Endo, F., Komine, O., Fujimori-Tonou, N., Katsuno, M., Jin, S., Watanabe, S., Sobue, G., Dezawa, M., Wyss-Coray, T., Yamanaka, K., 2015. Astrocyte-derived TGF-β1 accelerates disease progression in ALS mice by interfering with the neuroprotective functions of microglia and T cells. Cell Rep. 11, 592–604.

Engelhardt J.I., J. Tajti, S.H. Appel, Lymphocytic infiltrates in the spinal cord in amyotrophic lateral sclerosis. Arch Neurol. 1993 50(1):30-6 (1993).

Finkelstein A., Abnormal changes in NKT cells, the IGF-1 axis, and liver pathology in an animal model of ALS. *PLoS One* 6(8), e22374, 2011.

Foran, E., Bogush, A., Goffredo, M., Roncaglia, P., Gustincich, S., Pasinelli, P., Trotti, D., 2011. Motor neuron impairment mediated by a sumoylated fragment of the glial glutamate transporter EAAT2. Glia 59, 1719–1731.

Frakes, A.E., Ferraiuolo, L., Haidet-Phillips, A.M., Schmelzer, L., Braun, L., Miranda, C.J., Ladner, K.J., Bevan, A.K., Foust, K.D., Godbout, J.P., Popovich, P.G., Guttridge, D.C., Kaspar, B.K., 2014. Microglia induce motor neuron death via the classical NF-κB pathway in amyotrophic lateral sclerosis. Neuron 81, 1009–1023.

Gan, Y., Liu, R., Wu, W., Bomprezzi, R., Shi, F.D., 2012. Antibody to α4 integrin suppresses natural killer cells infiltration in central nervous system in experimental autoimmune encephalomyelitis. J. Neuroimmunol. 247, 9–15.

Garbuzova-Davis, S., Hernandez-Ontiveros, D.G., Rodrigues, M.C., Haller, E., Frisina-Deyo, A., Mirtyl, S., Sallot, S., Saporta, S., Borlongan, C.V., Sanberg, P.R., 2012. Impaired blood-brain/spinal cord barrier in ALS patients. Brain Res. 21 (1469), 114–128. https://doi.org/10.1016/j.brainres.2012.05.056.

Garbuzova-Davis S., S. Saporta, E. Haller, I. Kolomey, S.P. Bennett, H. Potter, P.R. Sanberg, Evidence of compromised blood-spinal cord barrier in early and late symptomatic SOD1 mice modeling ALS. *PLoS One* 21;2(11):e1205 (2007). doi: 10.1371/journal.pone.0001205.

Garofalo, S., Cocozza, G., Porzia, A., Inghilleri, M., Raspa, M., Scavizzi, F., Aronica, E., Bernardini, G., Peng, L., Ransohoff, R.M., Santoni, A., Limatola, C., 2020. Natural killer cells modulate motor neuron-immune cell cross talk in models of Amyotrophic Lateral Sclerosis. Nat. Commun. 11, 1173.

Gate, D., Tapp, E., Leventhal, O., Shahid, M., Nonninger, T.J., Yang, A.C., Strempfl, K., Unger, M.S., Fehlmann, T., Oh, H., Channappa, D., Henderson, V.W., Keller, A., Aigner, L., Galasko, D.R., Davis, M.M., Poston, K.L., Wyss-Coray, T., 2021. CD4+ T cells contribute to neurodegeneration in Lewy body dementia. Science 374 (6569), 868–874.

Gong, Y.H., Parsadanian, A.S., Andreeva, A., Snider, W.D., Elliott, J.L., 2000. Restricted expression of G86R Cu/Zn superoxide dismutase in astrocytes results in astrocytosis but does not cause motoneuron degeneration. J. Neurosci. 20, 660–665.

Guidotti, G., Scarlata, C., Brambilla, L., Rossi, D., 2021. Tumor necrosis factor alpha in amyotrophic lateral sclerosis: friend or foe? Cells 10, 518.

Haidet-Phillips, A.M., Hester, M.E., Miranda, C.J., Meyer, K., Braun, L., Frakes, A., Song, S., Likhite, S., Murtha, M.J., Foust, K.D., Rao, M., Eagle, A., Kammesheidt, A., Christensen, A., Mendell, J.R., Burghes, A.H., Kaspar, B.K., 2011. Astrocytes from familial and sporadic ALS patients are toxic to motor neurons. Nat. Biotechnol. 29, 824–828.

Hatzipetros, T., Bogdanik, L.P., Tassinari, V.R., Kidd, J.D., Moreno, A.J., Davis, C., Osborne, M., Austin, A., Vieira, F.G., Lutz, C., Perrin, S., 2014. C57BL/6J congenic Prp-TDP43A315T mice develop progressive neurodegeneration in the myenteric plexus of the colon without exhibiting key features of ALS. Brain Res. 10 (1584), 59–72.

Hemmer, B., Kerschensteiner, M., Korn, T., 2015. Role of the innate and adaptive immune responses in the course of multiple sclerosis. Lancet Neurol. 14 (4), 406–419.

Henkel, J.S., Beers, D.R., Wen, S., Rivera, A.L., Toennis, K.M., Appel, J.E., Zhao, W., Moore, D.H., Powell, S.Z., Appel, S.H., 2013. Regulatory T-lymphocytes mediate amyotrophic lateral sclerosis progression and survival. EMBO Mol. Med. 5 (1), 64–79.

Herdewyn, S., Cirillo, C., Van Den Bosch, L., Robberecht, W., Vanden Berghe, P., Van Damme, P., 2014. Prevention of intestinal obstruction reveals progressive neurodegeneration in mutant TDP-43 (A315T) mice. Mol. Neurodegener. 9 (1).

Hounoum, B.M., Mavel, S., Coque, E., Patin, F., Vourc'h, P., Marouillat, S., Nadal-Desbarats, L., Emond, P., Corcia, P., Andres, C.R., Raoul, C., Blasco, H., 2017. Wildtype motoneurons, ALS-Linked SOD1 mutation and glutamate profoundly modify astrocyte metabolism and lactate shuttling. Glia 65, 592–605.

Jones, Kathryn J, et al., Amy E Lovett-Racke, Chandler L Walker, Virginia M Sanders, 2015. CD4 + T Cells and Neuroprotection: Relevance to Motoneuron Injury and Disease. J Neuroimmune Pharmacol. 10(4), 587–594. https://doi.org/10.1007/s11481-015-9625-x.

Kang, S.H., Li, Y., Fukaya, M., Lorenzini, I., Cleveland, D.W., Ostrow, L.W., Rothstein, J. D., Bergles, D.E., 2013. Degeneration and impaired regeneration of gray matter oligodendrocytes in amyotrophic lateral sclerosis. Nat. Neurosci. 16, 571–579.

Kawamata, T., Akiyama, H., Yamada, T., McGeer, P.L., 1992. Immunologic reactions in amyotrophic lateral sclerosis brain and spinal cord tissue. Am. J. Pathol. 140 (3), 691–707.

Li, D., Liu, X., Liu, T., Liu, H., Tong, L., Jia, S., Wang, Y.F., 2020. Neurochemical regulation of the expression and function of glial fibrillary acidic protein in astrocytes. Glia 68, 878–897.

Linnerbauer, M., Wheeler, M.A., Quintana, F.J., 2020. Astrocyte crosstalk in CNS inflammation. Neuron 108 (4), 608–622.

Liu, J., Wang, F., 2017. Role of neuroinflammation in amyotrophic lateral sclerosis: cellular mechanisms and therapeutic implications. Front. Immunol. 21, 8:1005.

Liu, Z., Cheng, X., Zhong, S., Zhang, X., Liu, C., Liu, F., Zhao, C., 2020. Peripheral and central nervous system immune response crosstalk in amyotrophic lateral sclerosis. Front. Neurosci. 16, 14:575.

Ludolph A., V. Drory, O. Hardiman, I. Nakano, J. Ravits, W. Robberecht, J. Shefner, WFN Research Group On ALS/MND. A revision of the El Escorial criteria *Amyotroph Lateral Scler Frontotemporal Degener.* 16(5-6), 291-2 (2015).

Mäkelä, J., Koivuniemi, R., Korhonen, L., Lindholm, D., 2010. Interferon-gamma produced by microglia and the neuropeptide PACAP have opposite effects on the viability of neural progenitor cells. PLoS ONE 5 (6), e11091.

McGeer, P.L., McGeer, E.G., 2002. Inflammatory processes in amyotrophic lateral sclerosis. Muscle Nerve 26 (4), 459–470.

Murdock, B.J., Zhou, T., Kashlan, S.R., Little, R.J., Goutman, S.A., Feldman, E.L., 2017. Correlation of peripheral immunity with rapid amyotrophic lateral sclerosis progression. JAMA Neurol. 74 (12), 1446.

Nahirney, P.C., Tremblay, M.E., 2021. Brain ultrastructure: putting the pieces together. Front. Cell Dev. Biol. 18, 9:629503.

Nardo, G., Trolese, M.C., Verderio, M., Mariani, A., de Paola, M., Riva, N., Dina, G., Panini, N., Erba, E., Quattrini, A., Bendotti, C., 2018. Counteracting roles of MHCI and $CD8^+$ T cells in the peripheral and central nervous system of ALS $SOD1^{G93A}$ mice. Mol. Neurodegener. 13 (1), 42. https://doi.org/10.1186/s13024-018-0271-7.

Parisi, C., Arisi, I., D'Ambrosi, N., Storti, A.E., Brandi, R., D'Onofrio, M., Volonté, C., 2013. Dysregulated microRNAs in amyotrophic lateral sclerosis microglia modulate genes linked to neuroinflammation. Cell Death Dis. 12, e959.

Peric, M., Mitrecic, D., Andjus, P.R., 2017. Targeting astrocytes for treatment in amyotrophic lateral sclerosis. Curr. Pharm. Des. 23, 5037–5044.

Philips, T., Robberecht, W., 2011. Neuroinflammation in amyotrophic lateral sclerosis: role of glial activation in motor neuron disease. Lancet Neurol. 10 (3), 253–263.

Rock, R.B., Hu, S., Deshpande, A., Munir, S., May, B.J., Baker, C.A., Peterson, P.K., Kapur, V., 2005. Transcriptional response of human microglial cells to interferon-gamma. Genes Immun. 6, 712–719.

Savage, J.C., St-Pierre, M.K., Carrier, M., El Hajj, H., Novak, S.W., Sanchez, M.G., Cicchetti, F., Tremblay, M.E., 2020. Microglial physiological properties and interactions with synapses are altered at presymptomatic stages in a mouse model of Huntington's disease pathology. J. Neuroinflamm. 17, 98.

Smith, B.C., Sinyuk, M., Jenkins 3rd, J.E., Psenicka, M.W., Williams, J.L., 2020. The impact of regional astrocyte interferon-γ signaling during chronic autoimmunity: a novel role for the immunoproteasome. J. Neuroinflamm. 17 (1), 184.

Spiller, K.J., Restrepo, C.R., Khan, T., Dominique, M.A., Fang, T.C., Canter, R.G., Roberts, C.J., Miller, K.R., Ransohoff, R.M., Trojanowski, J.Q., Lee, V.-Y., 2018. Lee V.M., Microglia-mediated recovery from ALS-relevant motor neuron degeneration in a mouse model of TDP-43 proteinopathy. Nat. Neurosci. 21 (3), 329–340.

Stephenson, J., Nutma, E., van der Valk, P., Amor, S., 2018. Inflammation in CNS neurodegenerative diseases, Inflammation in CNS neurodegenerative diseases. Immunology 154 (2), 204–219.

St-Pierre M.K., E. Šimončičová, E. Bögi, M.E. Tremblay, Shedding Light on the Dark Side of the Microglia. *ASN Neuro.* 12, 1759091420925335 (2020).

Thonhoff, J.R., Gao, J., Dunn, T.J., Ojeda, L., Wu, P., 2011. Mutant SOD1 microglia-generated nitroxidative stress promotes toxicity to human fetal neural stem cell-derived motor neurons through direct damage and noxious interactions with astrocytes. Am. J. Stem Cells 19, 2–21.

Troost, D., van den Oord, J.J., de Jong, J.M., Swaab, D.F., 1989. Lymphocytic infiltration in the spinal cord of patients with amyotrophic lateral sclerosis. Clin. Neuropathol. 8, 289–294.

Unger, M.S., Li, E., Scharnagl, L., Poupardin, R., Altendorfer, B., Mrowetz, H., Hutter-Paier, B., Weiger, T.M., Heneka, M.T., Attems, J., Aigner, L., 2020. $CD8^+$ T-cells infiltrate Alzheimer's disease brains and regulate neuronal- and synapse-related gene expression in APP-PS1 transgenic mice. Brain Behav. Immun. 89, 67–86.

Vahsen, B.F., Gray, E., Thompson, A.G., Ansorge, O., Anthony, D.C., Cowley, S.A., Talbot, K., Turner, M.R., 2021. Non-neuronal cells in amyotrophic lateral sclerosis - from pathogenesis to biomarkers. Nat. Rev. Neurol. 6, 333–348.

Zamudio, F., Loon, A.R., Smeltzer, S., Benyamine, K., Navalpur Shanmugam, N.K., Stewart, N.J.F., Lee, D.C., Nash, K., Selenica, M.-L., 2020. TDP-43 mediated blood-brain barrier permeability and leukocyte infiltration promote neurodegeneration in a low-grade systemic inflammation mouse model. J. Neuroinflammation. 17 (1).

Wang, L., Gutmann, D.H., Roos, R.P., 2011. Astrocyte loss of mutant SOD1 delays ALS disease onset and progression in G85R transgenic mice. Hum. Mol. Genet. 20, 286–293.

Wegorzewska, I., Bell, S., Cairns, N.J., Miller, T.M., Baloh, R.H., 2009. TDP-43 mutant transgenic mice develop features of ALS and frontotemporal lobar degeneration. Proc. Natl. Acad. Sci. U.S.A. 106, 18809–18814.

Yang, Z., Wang, K.K., 2015. Glial fibrillary acidic protein: from intermediate filament assembly and gliosis to neurobiomarker. Trends Neurosci. 38 (6), 364–374.

Yu, Y., Schürpf, T., Springer, T.A., 2013. How natalizumab binds and antagonizes α4 integrins. J. Biol. Chem. 45, 32314–32325.